

An Explanation for the Different X-ray to Optical Column Densities in the Environments of Gamma Ray Bursts: A Progenitor Embedded in a Dense Medium

Yair Krongold¹ and J. Xavier Prochaska²

ABSTRACT

We study the $\gtrsim 10$ ratios in the X-ray to optical column densities inferred from afterglow spectra of Gamma Ray Bursts due to gas surrounding their progenitors. We present time-evolving photoionization calculations for these afterglows and explore different conditions for their environment. We find that homogenous models of the environment (constant density) predict X-ray columns similar to those found in the optical spectra, with the bulk of the opacity being produced by neutral material at large distances from the burst. This result is independent of gas density or metallicity. Only models assuming a progenitor immersed in a dense ($\sim 10^{2-4} \text{ cm}^{-3}$) cloud of gas (with radius $\sim 10 \text{ pc}$), with a strong, declining gradient of density for the surrounding interstellar medium are able to account for the large X-ray to optical column density ratios. However, to avoid an unphysical correlation between the size of this cloud, and the size of the ionization front produced by the GRB, the models also require that the circumburst medium is already ionized prior to the burst. The inferred cloud masses are $\lesssim 10^6 M_{\odot}$, even if low metallicities in the medium are assumed ($Z \sim 0.1 Z_{\odot}$). These cloud properties are consistent with those found in giant molecular clouds and our results support a scenario in which the progenitors reside within intense star formation regions of galaxies. Finally, we show that modeling over large samples of GRB afterglows may offer strong constraints on the range of properties in these clouds, and the host galaxy ISM.

Subject headings:

¹Instituto de Astronomia, Universidad Nacional Autonoma de Mexico, Apartado Postal 70-264, 04510 Mexico DF, Mexico.

²Department of Astronomy and Astrophysics, UCO/Lick Observatory; University of California, 1156 High Street, Santa Cruz, CA 95064; xavier@ucolick.org

1. Introduction

GRBs are the most powerful sources of radiation in the Universe. Although they shine for brief periods of time, their afterglows are capable of ionizing their surrounding material to large distances – tens to hundreds of pc (Perna & Loeb 1998; Perna & Lazzati 2002a; Prochaska et al. 2008; Piranomonte et al. 2008; D’Elia et al. 2009a). Therefore, GRB afterglows can ionize the medium close to the progenitor, the region of star formation containing the progenitor, and even part of the inter-stellar medium (ISM) of the host galaxy. Furthermore, as the light travels along our line of sight, GRB afterglows “illuminate” the host galaxy in absorption giving us a detailed view of the surrounding gas. As a result, GRBs have been used over the last decade as probes of the physical conditions of the ISM in distant galaxies (e.g. Savaglio 2006; Prochaska et al. 2007b). In addition, it has been established that GRBs probe different regions than Quasars (likely because GRBs originate in star-forming regions), making studies of the environments of both objects complementary to one another (Vreeswijk et al. 2004; Prochaska et al. 2007b).

The material around GRBs has been observed spectroscopically both at X-ray and optical/UV frequencies. There is clear evidence for intrinsic absorption due to high columns of material in the X-ray spectra for the majority of GRB afterglows (Butler et al. 2006; Watson et al. 2007; Campana et al. 2012). The measured opacities imply metal column densities gauged by oxygen of $N_{\text{O}}^{\text{X}} \approx 10^{19} \text{ cm}^{-2}$. For a solar metallicity, which is likely rare (Prochaska et al. 2007b; Savaglio et al. 2012), this implies an effective hydrogen column density $N_{\text{H}} \approx 10^{22} \text{ cm}^{-2}$. Optical/UV spectroscopy also reveals strong intrinsic absorption in a large fraction ($\approx 90\%$) of sightlines to GRBs (Savaglio et al. 2003; Prochaska et al. 2007a; Fynbo et al. 2009). From these data, one may estimate the column densities for oxygen from the measurements of unsaturated transitions of Si, S, and Zn assuming solar relative abundances. Typical values are $N_{\text{O}}^{\text{UV}} \approx 10^{18} \text{ cm}^{-2}$ with a large dispersion. One also measures, from damped H I Ly α absorption, neutral hydrogen column densities of $N_{\text{HI}} \approx 10^{21-22} \text{ cm}^{-2}$ (Jakobsson et al. 2006). These X-ray and optical/UV spectroscopic observations, each require a large reservoir of gas along the sightline, presumably tracing the circumburst medium and the larger-scale, ambient ISM of the galaxy.

However, when a direct comparison between the X-ray and optical inferred column densities toward individual GRBs has been possible, a discrepancy has been observed: the inferred column density of atoms and ions from X-ray studies are systematically larger (by factors of a few to several orders of magnitude) than the column densities measured in the optical/UV (Watson et al. 2007; Schady et al. 2011; Campana et al. 2012)¹. Since the ab-

¹Standard treatment in the literature is to recast these metal column densities as equivalent H column

sorption observed in the X-rays is sensitive to the total column density of material in the line of sight (produced from neutral atoms up to highly ionized, but not fully stripped species), while that in the optical/UV region depends on the ionization state of the gas (probing better absorption by cooler gas), it has been proposed that the discrepancies are the result of photoionization of the gas close to the GRB by its own radiation field (Watson et al. 2007; Schady et al. 2011). The large X-ray column densities also suggest a dense environment near the burst location (Campana et al. 2012) while analysis of fine-structure transitions in the optical/UV indicate the neutral gas lies at distances of ≈ 100 pc to many kpc (Prochaska et al. 2006; Dessauges-Zavadsky et al. 2006; Vreeswijk et al. 2007; D’Elia et al. 2009a; Sheffer et al. 2009).

While these are plausible hypotheses, quantitative work is required to explore the viability and implications for the circumburst medium and beyond. The principal challenge is to construct a physically realistic model with sufficient opacity in the ionized gas on small scales without over-predicting the observed column densities of lower ionization state gas. If the medium has roughly a constant density, the column density of the colder gas can easily supersede that of the ionized material even at low distances from the burst (see §4), suggesting the presence of an inhomogeneous distribution of material around the burst (with denser gas closer to the burst region).

In order to study the circumburst medium around GRBs, considering in a self-consistent manner both the gas distribution and its ionization structure, one must consider that the gas is far from ionization equilibrium after the onset of the burst (§2). As has been shown by calculations carried out in the past, following the time evolution of the ionization state of the gas is required to obtain reliable models of the surrounding material. This has been amply demonstrated by Lazzati & Perna (2002), Perna & Lazzati (2002b), Perna et al. (2003), and Lazzati & Perna (2003). These authors present observable constraints on the X-ray versus Optical (dust continuum) extinction, based on self-consistent models considering time evolving calculations for both the dust fraction and the ionization state of the gaseous phase. Special attention is put on the effects of dust on the medium. More recently, Prochaska et al. (2008) have studied the time effects on the ionization structure and front in the circumburst medium (see also Piranomonte et al. 2008; D’Elia et al. 2009a,b). These studies have been valuable in determining the effects of the GRB in their medium, however, they have not attempted to explain the different column densities explained above, and have assumed homogeneous gas distributions.

As a first step to further explore these differences, we have used a custom time-dependent

densities, but that is not necessary nor preferred for the following analysis.

photoionization code to predict the relative column densities of gas relevant to X-ray and optical/UV observations. The code computes the evolution of the different ionization species as a function of time and distance, given the luminosity, light curve, and spectral energy distribution of a source emitting ionizing photons. To focus the discussion, we compare results obtained so far in the literature against a fiducial model representative of the medium surrounding GRBs. These tend to show an excess of ~ 10 in column density between the X-ray and optical spectra of the source.

The paper is organized as follows: In §2 we describe briefly the code and provide a test case to exemplify in a simple way the time evolution of the circumburst medium. In §3 we lay out the assumptions for the particular fiducial models presented here. In §4 we present and analyze our results. Finally, §5 summarizes our findings. Throughout the paper we have assumed a Hubble constant $H_0=72 \text{ km s}^{-1} \text{ Mpc}^{-1}$, a dark energy fraction $\Omega_\Lambda=0.75$, and a matter fraction $\Omega_m=0.25$.

2. Time-Evolving Photoionization Calculations

GRB afterglows have roughly a power-law spectrum (due to synchrotron processes), with emission extending from X-ray to radio frequencies. Therefore, the emission of GRB afterglows contains a large fraction of ionizing photons that will ionize and heat the surrounding material. These photons will produce an ionization front, that will expand over time as additional radiation impinges on the gas. An ionization structure is expected around the burst, with highly ionized material near the burst and progressively less ionized gas farther out, owing to the geometrical dilution of the radiation field, the finite propagation time of the ionization front, and the opacity of the circumburst medium. The ionization structure is also time-dependent, as both the GRB flux and the integrated opacity of the gas evolve.

To model the behavior of the ionization front and structure with time, we have performed a series of time-evolving photoionization calculations using a code developed originally to measure the evolution of ionized gas near Active Galactic Nuclei. The code solves a set of linear differential equations that describe the evolution of the abundance of the different ions n_i as a function of the variation of the incident flux with time, and as a function of the ionization and recombination processes (that also are time dependent). For a detailed discussion on time evolving photoionization processes we refer the reader to Nicastro et al. (1999) and Krongold et al. (2007).

The code calculates the ionic abundances as a function of time for H and He, as well as for heavier elements, namely C, N, O, Ne, Mg, Al, Si, S, and Fe. It includes first order

radiation transfer, as the impinging radiation is attenuated by a series of optically thin layers of material (with thickness $\sim 10^{16}$ cm for $n_{\text{H}} = 1 \text{ cm}^{-3}$), and is diluted by geometry. The code does not include diffuse radiation (due to recombinations) in the radiative transfer calculations (although they are included in the time evolution of the ionic species). This is a good approximation in the case of the material around GRB afterglows because the expected densities in these regions ($\ll 10^6 \text{ cm}^{-3}$) imply recombination times much longer than the duration of the burst. For the conditions in this gas, the recombination time ranges from tens to thousands of years (to first order, the recombination time is inversely proportional to the number density of atoms in the gas).

The code solves the time evolution in the first parcel of gas for the whole light curve, then it uses the attenuated (time-dependent) flux exiting this shell as the impinging flux for the next one. This procedure is repeated until the ionization fraction is calculated at all times up to a given distance. In our calculations we have produced models up to 100 pc from the ionizing source. We only consider distances larger than 1pc from the burst location. This has the advantage of reducing considerably the computing time of the models. At closer distances, the medium is completely stripped by the GRB radiation only a few seconds after the onset. A full description of the code will be given in a forthcoming paper (Krongold et al. 2013). Calculations using this code have previously been presented for intrinsic absorption observed in the line of sight to GRB 080330 (D’Elia et al. 2009a), GRB080319B (D’Elia et al. 2009b), and GRB050922C (Piranomonte et al. 2008).

As a simple test case, we present models for GRB 050730 and compare against an analagous calculation by Prochaska et al. (2008). The calculations were performed using the same parameters reported by these authors, namely, the luminosity of ionizing photons, the light curve, and the spectral energy distribution (SED) of the GRB afterglow, as well as the gas density (which is assumed to be homogeneous with $n_{\text{H}} = 10 \text{ cm}^{-3}$). Figure 1a (left panel) presents our results. The similarities between the ionization structure predicted by our model (left panel in the Fig.) and the one calculated by Prochaska et al. (Fig. 3 in their paper) at 1000 seconds after the burst are reassuring. This figure also reveals the stratification of ionization states within the surrounding medium. In particular, it can be observed that the higher ionization charge states are formed closer to the source, up to a distance ~ 15 pc away from the burst, where the ionization front is located.

In Figure 1b (right panel), we illustrate the time evolution for several ions. In particular those high ionization ions that can be more easily observed in the UV/Optical spectra of GRBs, as well as OVII, which is a natural tracer of the highly ionized gas that may provide a significant X-ray opacity. During the first few thousand seconds (observer frame time), gas up to 5-10 pc away from the burst can reach a high level of ionization (showing states such

as N V, O VI). At tens of kiloseconds, similar ionization conditions would be driven to even larger distances (tens of pc). At these times, the gas closer to the GRB will no longer be observed in these ions because the gas will be driven to even higher ionization states (e.g. N VI, O VII, O VIII) that are not observed in UV/optical spectra but instead in X-rays. This plot exemplifies, in a simple way, the expected time evolution of the ionization structure near the GRB.

We note in passing that observations of GRB afterglows are typically carried out several hours (kiloseconds to tens of kiloseconds) after the burst. Thus, if the hot gas is indeed photoionized by the afterglow, observations of highly ionized gas do trace the close environment of the GRB, which may include the circumstellar medium of the progenitor star and/or the star forming region where it was embedded.

3. A Fiducial GRB Model

Long-duration GRBs show a significant diversity in their spectral properties and in the characteristics of intrinsic absorption imprinted on their afterglows. In a future work, we intend to explore this diversity to infer variations in properties of the circumburst medium. In this manuscript, we focus on the specific challenge of the set of GRBs which exhibit strong X-ray absorption with more modest absorption in the optical/UV. It is illustrative, of course, to consider the problem quantitatively. To that end, we consider a fiducial model for a GRB event which is representative of many GRBs. Our fiducial model (described below) is based on the average properties of the sample of Swift GRBs presented by Margutti et al. (2013) for which data of the prompt and afterglow emission has been analyzed.

3.1. GRB Emission

The GRB emission is characterized by a light curve which tracks the time-evolution of the luminosity and a spectral energy distribution (SED) that may also vary with time. The X-ray light curve can be described in general by two two different phases (e.g. Willingale et al. 2007). Each phase is frequently modeled and observed to follow a broken power-law $L \propto t^\alpha$. The first phase (hereafter referred as the prompt phase) is strongly related to the prompt γ -ray emission, and consists of a nearly constant emission followed by a steep decay (Tagliaferri et al. 2005; Goad et al. 2006). In the second phase (hereafter the afterglow phase) the light curve flattens and then follows a “normal decay” (the break in this phase is generally interpreted as the shock break-out, i.e. the time when the size of the relativistic

beam matches the physical extent of the jet).

In the following, we model the prompt phase considering a constant emission up to $t_p = 85$ s after the burst followed by a steep decay described by $\alpha_1 = -2.0$. We consider the transition between the prompt and afterglow phases to occur at $t_b = 100$ s. From this time on, we model the afterglow light curve by a power-law with $\alpha_2 = -1.0$. We do not model the break in the second phase from flat to “normal” decay. This break usually involves a small change in slope and takes place at later times, when the bulk of the photons has already been emitted. Thus it has little effect in our results. Our choice of α_2 and t_b is based on the average values found by Margutti et al. (2013). The rest of the parameters were constrained to match the average luminosities found for GRBs by these same authors (see below).

Although the GRB emission is believed to be dominated by synchrotron emission, its SED is both predicted and observed to be relatively complex (Sari et al. 1998). One often models it as a series of power-laws $L_\nu \propto \nu^{-\beta}$ across the electromagnetic spectrum. Our photoionization modeling, however, is only sensitive to the SED at rest-frame energies from 1 Ryd to 100 keV, i.e. the UV to X-ray passbands. Therefore we model the SED as a single power-law. We note however, that there can be strong spectral evolution between the prompt and afterglow phases of the light curve and that the early SED has not been studied systematically. However, studies of individual cases show a much harder slope than that in the afterglow (e.g. Butler et al. 2006; Stratta et al. 2009). In the following we assume $\beta = 0.0$ in the prompt phase (before $t_b = 100$ s) and $\beta = 1.0$ for the afterglow.

Lastly, we have set the afterglow luminosity. We consider a total X-ray energy $E_{X,iso} = 4.1 \times 10^{51}$ erg integrated between 0.3 – 10.0 keV and from $t = 0$ s to $t = 10^4$ s. The amount of X-ray energy released in the prompt phase is $E_{X,pt} = 1.4 \times 10^{51}$ erg and that in the afterglow is $E_{X,ag} = 2.7 \times 10^{51}$ erg. These values are representative of the Swift GRB sample by Margutti et al. (2013). With these considerations, the total amount of ionizing photons emitted by this fiducial GRB is $\phi_o = 2.1 \times 10^{61}$ ph up to $t = 10^4$ s.

3.2. Absorption of the GRB Afterglow

We compare the circumburst models ionized by the above afterglow to a characteristic set of measurements for gas column densities from analysis of X-ray and optical/UV afterglow spectroscopy. Giving that the equivalent H column density obtained from the X-rays and the column density of neutral material obtained from the optical spectrum were derived assuming solar abundances (the neutral column density assumes solar abundances as it was measured from metals, not HI), we compare the results of our models not to H, but rather to

O. Analysis of those GRBs exhibiting significant X-ray opacity typically yield estimates for the effective hydrogen column densities of $N_{\text{H}} \approx 10^{22} \text{ cm}^{-2}$ (Watson et al. 2007; Schady et al. 2011; Campana et al. 2012). These values were derived by assuming solar abundances² and a fully neutral medium. The implied column densities of oxygen therefore scale as 7×10^{-4} , giving $N_{\text{O}}^{\text{X}} \approx 10^{19} \text{ cm}^{-2}$. We adopt this as our fiducial value for a typical GRB showing X-ray absorption.

Regarding the optical/UV spectroscopy, the commonly observed O I transitions are always saturated and one can only estimate N_{O}^{UV} by scaling measurements of non-refractory elements (e.g. S, Si, Zn) assuming solar relative abundances. Values from the literature range from $N_{\text{O}}^{\text{UV}} = 10^{16-18.5} \text{ cm}^{-2}$. As emphasized in the Introduction, a significant fraction of GRBs with X-ray absorption show $N_{\text{O}}^{\text{X}} \approx 10 N_{\text{O}}^{\text{UV}}$ (Schady et al. 2011). In the following, we adopt $N_{\text{O}}^{\text{UV}} = 10^{18} \text{ cm}^{-2}$ as our fiducial value.

Given that we will explore the conditions required to measure (much) larger columns in the X-rays than in the optical, and these conditions are likely due to ionization, we will evaluate our models considering that the observed X-ray column density is produced mainly by the ionized gas, while the optical column is produced by the neutral one. As will be clear from the models, this is indeed the case, and any contribution from the neutral material to the X-ray absorption is negligible if larger columns in this spectral region are required. Although we run models with many different conditions, we report here only the most relevant to explain the observations.

4. Results and Discussion

4.1. Uniform Models of the Circum-Burst Medium

We begin by examining the time-dependent results from a series of idealized models with constant gas density extending to a circumburst radius $r_{\text{CBM}} = 150 \text{ pc}$. Calculations at larger locations are not required given that the ionization front for all models takes place inside this distance. Within this model framework, we explore a range of gas density ($n = 10$ and $n = 10^3 \text{ cm}^{-3}$) and metallicity ($Z = Z_{\odot}$ and $Z = 0.01 Z_{\odot}$). Figure 2 shows the radius, as a function of time, to two transition regions driven by the afterglow for a series of models. These two transition regions are: (i) r_{HI} , the radius at which the gas has a 50% hydrogen

²The authors do not report the O abundance assumed in their models. However their models were carried out using Xspec. The standard abundances on Xspec can be varied according to different measurements, but all are consistent with the O abundance assumed here within a factor ~ 1.5 .

neutral fraction; and (ii) r_{OIX} , the radius at which the gas has 90% of its oxygen completely stripped of electrons. These define the neutral region ($r > r_{\text{HI}}$) within the ambient medium which dominates the UV opacity, and the start of the ionized region ($r = r_{\text{OIX}}$) where the X-ray bound-free and bound-bound opacity begins. Both radii have a power-law dependence during the prompt phase emission ($t < t_b = 100$ s). At t_b the afterglow emission begins and the radiation impinging on the gas becomes much softer ($\beta = 1.0$). This produces a rapid raise in r_{HI} right after t_b , due to the larger number of UV photons. At later times ($t > 500$ s) both r_{OIX} and r_{HI} follow a power-law again, but with a different slope.

It is evident from the plot that there is relatively weak dependence of the radii with metallicity as these are set by either the density of the gas or the r^{-2} dilution of the flux. One also notes that the evolution of r_{OIX} is weakly dependent on the density. This is because the gas is never optically thick to photons that ionize O^{+8} and r_{OIX} is mainly set by r^{-2} geometrical dilution of the afterglow. Each r_{OIX} curve reaches ≈ 3 pc at $t = 10^4$ s, indicating the gas in the inner few pc cannot contribute to the observed X-ray opacity. In contrast, r_{HI} has a different evolution for the models considered. For models with higher density, the ionization front lies closer to the source owing to the greater opacity of the medium. Due to this larger opacity, in these models r_{OIX} can even be larger than r_{HI} for the few tens of seconds after the burst. This unusual ionization structure, where O IX can exist in the neutral H region is due to the very hard SED of the prompt emission phase.

In Figure 3, we present the cumulative column densities of ionized (solid) and neutral (dotted) oxygen at $t = 1000$ s for a series of models. It is important to note that the ionized columns include only the contribution from charge states with at least one bound electron, e.g. O IX is not included. Under the assumption that the ionized gas must dominate the X-ray opacity, we require values of $N_{\text{O}}^{\text{X}} \approx 10^{19} \text{ cm}^{-2}$. It is evident from Figure 3 that this requires a very high density ($n_{\text{H}} > 10^2 \text{ cm}^{-3}$), even when one adopts a solar metallicity. If the large column densities observed in the X-ray spectra of GRB afterglows are indeed due to ionized material by the burst, then the densities and/or metallicities of the circumburst gas must be very large. Alternatively, one could reproduce the observed N_{O}^{X} values with neutral gas with much lower density extending to circumburst distances $r_{\text{CBM}} \gg 100$ pc. This would imply $N_{\text{O}}^{\text{UV}} \approx N_{\text{O}}^{\text{X}}$ which is inconsistent with the observations.

An additional interesting point is obvious when comparing the model with $Z = 0.01 Z_{\odot}$ and $n = 10^3 \text{ cm}^{-3}$ with that having $Z = Z_{\odot}$ and $n = 10 \text{ cm}^{-3}$. Although the ionization front takes place at different distances (Figure 2), the column densities inferred for ionized O have similar values within a factor of a few. This is expected, as the total column density of O depends almost linearly on both metallicity and density. However, without an a-priori knowledge of where the ionization front takes place (as is the case with spectroscopic

observations of GRBs), there is a degeneracy between the metallicity and the density of the material. Because of this, we will discuss models for solar metallicity in the rest of the paper, and will present those with different metallicities when appropriate.

A uniform prediction of these constant density models is that the column density of neutral material matches or even exceeds the ionized phase within the first 100 pc from the burst. This follows from the fact that $r_{\text{HI}} \lesssim 20 \text{ pc}$ (Figure 2) such that the medium is dominated by neutral gas along any given sightline. Integrating to $r = 100 \text{ pc}$, all the models predict larger columns of neutral than ionized O (by at least a factor of a few). As such, one predicts column densities probed by X-rays that exceed the optical/UV by only as much as 50% ($N_{\text{O}}^{\text{X}} < 1.5N_{\text{O}}^{\text{UV}}$). We note that it is likely that the ISM of the host galaxy extends further beyond the first 100 pc from the burst, making the X-ray and optical/UV columns even more similar. This violates the constraints of our fiducial afterglow model where $N_{\text{O}}^{\text{X}} \sim 10N_{\text{O}}^{\text{UV}}$. Thus, unless the circumburst medium has size $r_{\text{CBM}} \ll 100 \text{ pc}$, this model contradicts what is frequently observed. In this case, the bulk of the opacity (in both wavelength ranges) would be dominated by neutral material. We conclude that if the large columns found in the X-rays are indeed due to material ionized by the GRB afterglow, then the density and metallicity should be large, and the distribution of material cannot be homogeneous.

Given that the the progenitors of long GRBs might be massive stars with stellar winds (Woosley 1993), possibly embedded in intense star-forming regions, we must consider the possibility that the material within a few tens of pc from the progenitor was ionized prior to the onset of the burst. Indeed, simple treatments of likely progenitors for GRBs predict such ‘pre-ionization’ (Perna & Lazzati 2002a; Whalen et al. 2008). Then, it is important to test how these conditions may affect the results presented above. We have produced a series of models varying r_{preion} , the radius to which the gas has been pre-ionized prior to the GRB event. We assume an initial ionization distribution consistent with gas ionized by radiation following the spectral energy distribution of a massive star ($M \sim 30M_{\odot}$) giving a H neutral fraction of $f(\text{HI}) \sim 10^{-5}$. For $r_{\text{CBM}} \approx 100 \text{ pc}$, values of $r_{\text{preion}} < 50 \text{ pc}$ yield very similar results to those models without pre-ionization, as can be seen in Figure 3 (magenta line). This is because, although the ionization front and the ionized columns of material are larger due to the effects of the pre-ionization, at distances $r \sim 2r_{\text{preion}}$ from the burst the neutral column becomes comparable to that of ionized material. We note that r_{preion} might actually be much larger, satisfying the condition $r_{\text{preion}} \approx r_{\text{CBM}} = 100 \text{ pc}$. In this case, the contribution to the total column density from the neutral material up to r_{CBM} would be negligible (given that this gas was already ionized by the progenitor). However, as before, at a distance $\sim 2r_{\text{preion}}$ the neutral material from the ISM of the host galaxy would contribute as much as the ionized material to the total column density, so that again $N_{\text{O}}^{\text{X}} \sim N_{\text{O}}^{\text{UV}}$. Then,

in order to have $N_{\text{O}}^{\text{X}} \sim 10N_{\text{O}}^{\text{UV}}$, the total optical path length from the burst location to the ending radius of the galaxy would have to be $\sim r_{\text{CBM}}$. While this might be indeed the case for a few GRBs, we consider this possibility unlikely, because it requires that most GRBs are located near the edge of their host galaxies contrary to observations (Bloom et al. 2002; Fruchter et al. 2006).

4.2. Circum-Burst Medium Models Including Gradients of Density

Homogeneous models predict similar column densities in the X-ray and the optical/UV domains, with the bulk of the opacity due to neutral material at distances larger than a few tens of pc from the GRB. Furthermore, high column densities of ionized material require a circumburst medium with large density (or metallicity). Motivated by these results, we have explored simple models with gradients of density as a possible explanation for the larger X-ray column densities. The models presented here assume larger densities close to the burst, decreasing outwards. We explore models with a step in the density: $n = n_1$ at $r \leq r_{\text{step}}$ and $n = n_2$ at $r > r_{\text{step}}$, with $n_1 > n_2$. In all models we assume $n_2 = 1 \text{ cm}^{-3}$. Although this model is overly simplistic, models with radial gradients in density give similar results.

Figure 4 presents our results. The most important difference with the homogeneous cases is that, in general, in the step function model the neutral column density can be, by design, much lower than that for the constant density models. This is clearly observed when comparing the models with $n_1 = 10^3 \text{ cm}^{-3}$ (blue and cyan lines in Fig. 4 and blue line in Fig. 3).

Indeed, some step function models do predict $N_{\text{O}}^{\text{X}} \sim 10N_{\text{O}}^{\text{UV}}$. For instance, a model with $n_1 = 10^3 \text{ cm}^{-3}$ and $r_{\text{step}} = 5 \text{ pc}$ produces X-ray and UV column densities similar to the fiducial afterglow values (blue line in Fig. 4). However, if the same model is considered, but with $r_{\text{step}} = 10 \text{ pc}$ (cyan line), then $N_{\text{O}}^{\text{X}} \sim N_{\text{O}}^{\text{UV}}$ and this condition is no longer satisfied. This is because in the second model $r_{\text{step}} > r_{\text{HI}}$, and the dense region can contribute significantly to the neutral absorption. In general, these models are only capable of producing larger columns in the X-rays than in the UV if $r_{\text{step}} \sim r_{\text{HI}}$. Since there is no physical reason to assume a relation between the size of the ionization radius (which depends on the GRB properties) and the size of the dense region, we conclude that these models cannot naturally explain the ensemble of observations. This motivates a further addition to the model.

4.3. Models Including Gradients of Density and Pre-Ionization in the Circum-Burst Medium

Finally, we explore models with gradients of density, considering that the medium surrounding the GRB was already ionized before the burst explosion. As discussed before, there are strong arguments to assume a pre-ionized medium (Perna & Lazzati 2002a; Whalen et al. 2008). We explore the same density distribution as in §4.2 ($n = n_1$ at $r \leq r_{\text{step}}$ and $n = n_2$ at $r > r_{\text{step}}$, with $n_1 > n_2$ and $n_2 = 1 \text{ cm}^{-3}$). To avoid cases where $r_{\text{step}} > r_{\text{HI}}$, which produce $N_{\text{O}}^{\text{X}} \sim N_{\text{O}}^{\text{UV}}$ (§4.2), we consider only models where the region of pre-ionized gas contains the dense cloud of material (that is $r_{\text{preion}} > r_{\text{step}}$). As before, we assume a H neutral fraction $f(\text{HI}) \sim 10^{-5}$. Figure 5 presents our results. There are two notable benefits in these models.

1. Given the pre-ionization condition, the column density of the ionized material is dominated by gas at $r < r_{\text{step}}$. Therefore, the value of N_{O}^{X} measured is determined by the density and size of the denser region.
2. The neutral column density is produced, by design, outside the denser region. Therefore, N_{O}^{UV} is systematically lower than the column of ionized gas, i.e. $N_{\text{O}}^{\text{X}} \gg N_{\text{O}}^{\text{UV}}$.

We find that a model with $n_1 = 10^3 \text{ cm}^{-3}$ and $r_{\text{step}} = 10 \text{ pc}$ present X-ray and UV column densities similar to the fiducial afterglow values. The cyan line in Figure 5 presents this model. This is not a unique solution, of course; many solutions are possible, with lower n_1 requiring larger r_{step} . However, the solutions must satisfy two important conditions: (1) $r_{\text{step}} \lesssim r_{\text{preion}} < r_{\text{HI}}$, so that there is no contribution from the dense region to the neutral column density, and (2) we require $r_{\text{step}} > r_{\text{OIX}}$ so that the GRB does not entirely ionize the dense medium that provides the X-ray opacity.

Within these restrictions, the values that can reproduce our observations are constrained to be in the ranges $30 \text{ pc} > r_{\text{step}} > 5 \text{ pc}$, and $10^4 \text{ cm}^{-3} > n_1 > 5 \times 10^2 \text{ cm}^{-3}$. Different solutions produce X-ray and optical/UV column densities much different than the ratio of 10 from our fiducial value. For instance, a model with $r_{\text{step}} = 20 \text{ pc}$ and $n_1 = 10^3 \text{ cm}^{-3}$ (blue line in Fig. 5) would easily produce two orders of magnitude larger column in the X-rays than in the optical/UV, as found in several objects (Campana et al. 2010). These restrictions also impose a minimum pre-ionization radius around the GRB progenitor (condition (1) above), regions with $r_{\text{preion}} \sim 20 - 30 \text{ pc}$ are enough to explain the observations (see Figure 5). We consider these values to be very conservative, since detailed modeling shows that the progenitor can pre-ionize the surrounding material at distances $\gtrsim 100 \text{ pc}$ (Whalen et al. 2008). We note that our results do not place much restriction on the value of n_2 (the only condition being to keep small the neutral column density). Assuming again that the neutral

gas in the ISM extends for at least ~ 100 pc beyond the circumburst region implies that $n_2 \lesssim 10 \text{ cm}^{-3}$.

Given that step function models are very simplistic, we have also computed models assuming a constant density up to a distance r_{step} from the burst, and a density law parameterized by a power-law ($n = n_o(r/r_{\text{step}})^{-\alpha}$) at larger distances. We find qualitatively similar results to the step models provided $\alpha \gtrsim 2$. These models also yield $N_{\text{O}}^{\text{X}} > N_{\text{O}}^{\text{UV}}$ for $r_{\text{step}} < 30$ pc.

We conclude that the different column densities found in the X-ray and optical/UV regimes of GRB afterglow spectra can be well explained by the presence of ionized material within a few tens of pc of the burst location. This requires that the GRBs are produced in dense clouds of material within the host galaxy, with column densities characteristic of molecular clouds, and that this material is ionized prior to the explosion (Whalen et al. 2008). Our results even permit ionized versus neutral column density ratios up to 2-3 orders of magnitude or more, as reported by Campana et al. (2010). We note that some evidence of evolution with cosmic time in the X-ray absorbing column has been reported in previous works (Campana et al. 2010; Behar et al. 2011). We plan to test different scenarios to explain this evolution in a forthcoming paper³.

4.4. Additional Considerations on Mass and Metallicity

An independent constraint on the metallicity of the medium surrounding the GRB may come from stellar evolutionary theory. In this theory, late-type massive stars, such as Wolf-Rayet stars, are considered the most likely progenitor candidates for GRBs (Woosley & Heger 2006). Furthermore, low metallicities ($Z \lesssim 0.1 - 0.3Z_{\odot}$) are preferred by the models to avoid the spindown of the stellar core Izzard et al. (2004); Yoon & Langer (2005); Woosley & Heger (2006). We note however, that it is possible that the circumburst medium of the GRB has been contaminated with metals by the progenitor (at least to some extent). Thus, an extremely low metallicity is not strictly required to reconcile stellar evolutionary results with those presented here. However, somewhat low metallicities may still be expected in the circumburst region, and thus they are definitely desirable in the models. We note that it is

³While our manuscript was in revision, we became aware of a recent work by Watson et al. (2013) suggesting that absorption by He II may be producing most of the X-ray column density, and may be responsible for its evolution. This idea requires a SED with a very hard X-ray to UV photon index ($\Gamma \sim -1$), much harder than what is usually observed in GRB afterglows. A full time-evolving photoionization model testing this idea is warranted.

possible to get large columns of ionized material with arbitrarily low metallicities, provided that the density of the clouds where the progenitors are embedded is large enough.

Nevertheless, large densities may imply unphysically large masses for the progenitor’s cloud. For the more massive model presented in Figure 5 (blue line), the implied mass for $r_{\text{step}} = 20\text{pc}$ is $\approx 10^6 M_{\odot}$. This mass is characteristic of molecular clouds within the Galaxy (Murray 2011). Even a circumburst medium with $Z = 0.1Z_{\odot}$ may match our fiducial value for N_{O}^{X} (red line in Fig. 3). Only if $Z \ll 0.1Z_{\odot}$ (e.g. GRB 050730 Chen et al. 2005) would one require significantly larger density ($n_1 > 10^4 \text{cm}^{-3}$, magenta line) and a correspondingly larger mass of the circumburst medium. To the best of the authors knowledge, no GRB has been detected with such a low metallicity medium which also shows significant X-ray opacity.

We conclude that the cloud’s radius, density, and mass required to explain the differences between the X-ray and optical/UV column densities may be large (particularly if low metallicities are also required), but are fully comparable with those found in giant molecular clouds. Thus, our results support a scenario where GRB’s explode in giant molecular clouds within their host galaxies (Campana et al. 2006; Prochaska et al. 2008; Campana et al. 2010). A statistical study with observations of a large number of GRBs, spanning a wide range of luminosities, as well as X-ray and optical column densities, is required to further explore the properties of these clouds.

4.5. Ionic Column Densities and Time Variability

Two key ingredients in testing any model of the circumburst medium around GRBs is to study (1) the column densities of individual charge states, and (2) the possible variability (or lack of it) in the overall absorption properties of the material. In the following, we only discuss step function models including a pre-ionized medium, as these are the only ones consistent with the different X-ray and optical/UV column densities. We note that models with gradients of density are more likely to produce variability than models with constant density, because a charge state that was produced within the dense medium surrounding the GRB at short times after the burst, might be produced outside this region at later times. This would result in strong changes in column density for that particular ion.

To exemplify this, in Figures 6, 7, and 8 we present the time evolution of the fraction of Si IV, C IV, and N V for two different models with $n_1 = 10^3 \text{cm}^{-3}$ and $Z = 0.1 Z_{\odot}$. In the left upper panel of the plots (where a model with $r_{\text{step}} = 15 \text{pc}$ is presented) one observes that 100 s after the burst, the vast majority of these ions are produced in the dense medium.

However, when the observed time is ~ 1000 s, they are fully produced at > 15 pc, in the low density regions. Between these two times, the column density of these charge states decreases rapidly, as the peak in their fractional distributions moves out from the dense region into the diffuse medium (see solid lines in the bottom panel of Figures 6, 7, and 8).

An important additional constraint on the structure of the dense clouds of gas is set by the measured column densities of N V, which traces more highly ionized gas. The UV transitions from this ion have thus far been observed to be unsaturated, with column densities $N(N^{+4}) \sim 10^{14} \text{ cm}^{-3}$ (e.g. Prochaska et al. 2008, Fox et al. 2008). This implies that N V must be produced outside of the dense regions during these observations. In the case of our fiducial model, this means that the maximum allowed dense region size is $r_{\text{step}} = 15 - 20$ pc, because for larger sizes N V would be produced inside r_{step} even thousands of seconds after the burst, and the predicted column densities would be $\sim 100 - 1000$ times larger (see Fig. 8). However, we note that the GRBs where N V and other high ionization UV charge states can be observed are distant ($z \gtrsim 2$), and > 10 times brighter than our fiducial GRB luminosity (which is based on the average luminosity distribution by Margutti et al. (2013) and includes objects at all redshifts). Indeed, a model with 5 times more ionizing photons than our fiducial GRB produces N V at distances larger than 40 pc, only 1000 s after the burst (see upper right panel and dotted line in the bottom panel of Fig. 8). This makes possible much larger sizes for the dense region. In these bright GRBs, absorption from different charge states can be produced at large distances from the burst (hundreds of pc or more depending on the GRB luminosity), consistent with the observations (e.g. Fox et al. 2008). This is because of the much smaller opacity in a pre-ionized medium, with respect to a neutral one. Thus, pre-ionization is not only required to explain the large X-ray to optical/UV column density ratios, but also to explain absorption by photoionized elements at large distances from the GRB.

We remark that our models predict no variability in the total column densities of optical/UV observed charge states at times > 500 s, when the earliest spectroscopic observations in these wavebands are possible (e.g. Fox et al. 2008; D’Elia et al. 2009a). Our models, however, are not in contradiction with possible variations in individual charge states, as these can be produced by additional inhomogeneities in the diffuse medium, beyond r_{step} . These models are also consistent with the observations of variability in excited lines (e.g. Vreeswijk et al. 2007; D’Elia et al. 2009a), as these lines arise from material at large distances from the GRB region, in the ISM of the host galaxy. The spectral variations are produced by UV pumping from the GRB afterglow radiation into the excited levels of a single ion (e.g. Prochaska et al. 2006; D’Elia et al. 2009a) and not by variations in the total column density of that particular ion.

Finally, it is interesting to study how the total column density would vary with time. In Figure 9 we present the time evolution of the X-ray column density for the same models presented in Figure 5. The plot shows the expected variability for ionized O (excluding again O IX that does not contribute to the opacity). Only mild variations in the column density of ionized O should result in small variations in the measured column density in multi-time X-ray spectra of the afterglows. As it can be observed, the different step models predict variations by a factor $\lesssim 2$, according to their r_{step} . Variations by these factors cannot be measured in actual X-ray data (given the limited signal to noise ratio in the data and the uncertainties in the modeling). Nevertheless, a trend is expected with smaller columns found at larger times. Larger column density variations may be expected for GRBs embedded in smaller radii clouds (with $r_{\text{step}} \sim r_{\text{OIX}}=5 \text{ pc}$), as most of the gas cloud would be fully ionized at later times. However, this would also imply much smaller X-ray to Optical/UV column ratios at later times.

5. Summary and Future Work

In this work we present time-evolving photoionization calculations of the environments of GRBs. Our models indicate that the discrepancies found in the column density measurements carried out in the X-ray and optical/UV domains can be easily explained in terms of strong density gradients between the burst region, where the ionized X-ray absorption arises, and the extended (neutral) ISM of the host galaxy (imprinting absorption features in the optical/UV band). However, this requires that the dense medium surrounding the GRB is pre-ionized, as suggested by previous works.

Our results support a scenario in which the bursts are produced in dense condensations of material within their hosts. The masses, radii, and densities of these clouds are consistent with those found in giant molecular clouds, further implying that GRB are indeed produced within regions of intense star formation in galaxies. A case study for a fiducial GRB is too limited to further provide insights on the overall properties of such clouds (sizes, densities, masses, and metallicities distributions). However, here we show that time resolved spectroscopy of X-ray and Optical/UV data have strong diagnostic capabilities when compared to simple models. Producing detailed photoionization models –with physical parameters able to match the measured X-ray and optical column densities, for a large sample of bursts– is a promising way to shed light on the physical properties of the star formation regions where the GRB progenitors are born and evolve, and also on the ISM of their hosts.

We thank the anonymous referee for thoughtful comments that improved our paper and

Enrico Ramirez-Ruiz for insightful discussions. JXP acknowledges support from NASA/Swift grants NNX07AE94G and NNX12AD74G. YK acknowledges support from CONACyT 168519 grant and UNAM-DGAPA PAPIIT IN103712 grant. YK and JXP acknowledge support from a UC Mexus grant, FA 10-61.

REFERENCES

- Behar, E., Dado, S., Dar, A., & Laor, A. 2011, *ApJ*, 734, 26
- Bloom, J. S., Kulkarni, S. R., & Djorgovski, S. G. 2002, *aj*, 123, 1111
- Butler, N. R., et al. 2006, *ApJ*, 652, 1390
- Campana, S., et al. 2006, *A&A*, 449, 61
- . 2012, *MNRAS*, 421, 1697
- Campana, S., Thöne, C. C., de Ugarte Postigo, A., Tagliaferri, G., Moretti, A., & Covino, S. 2010, *MNRAS*, 402, 2429
- Chen, H.-W., Prochaska, J. X., Bloom, J. S., & Thompson, I. B. 2005, *ApJ*, 634, L25
- D’Elia, V., et al. 2009a, *ApJ*, 694, 332
- . 2009b, *A&A*, 503, 437
- Dessauges-Zavadsky, M., Chen, H.-W., Prochaska, J. X., Bloom, J. S., & Barth, A. J. 2006, *ApJ*, 648, L89
- Fox, A. J., Ledoux, C., Vreeswijk, P. M., Smette, A., & Jaunsen, A. O. 2008, *A&A*, 491, 189
- Fruchter, A. S., et al. 2006, *Nature*, 441, 463
- Fynbo, J. P. U., et al. 2009, *ApJS*, 185, 526
- Goad, M. R., et al. 2006, *A&A*, 449, 89
- Izzard, R. G., Ramirez-Ruiz, E., & Tout, C. A. 2004, *MNRAS*, 348, 1215
- Jakobsson, P., et al. 2006, *A&A*, 460, L13
- Krongold, Y., Nicastro, F., Elvis, M., Brickhouse, N., Binette, L., Mathur, S., & Jiménez-Bailón, E. 2007, *ApJ*, 659, 1022

- Lazzati, D., & Perna, R. 2002, MNRAS, 330, 383
- . 2003, MNRAS, 340, 694
- Margutti, R., et al. 2013, MNRAS, 428, 729
- Murray, N. 2011, ApJ, 729, 133
- Nicastro, F., Fiore, F., Perola, G. C., & Elvis, M. 1999, ApJ, 512, 184
- Perna, R., & Lazzati, D. 2002a, ApJ, 580, 261
- . 2002b, ApJ, 580, 261
- Perna, R., Lazzati, D., & Fiore, F. 2003, ApJ, 585, 775
- Perna, R., & Loeb, A. 1998, 501, 467
- Piranomonte, S., et al. 2008, A&A, 492, 775
- Prochaska, J. X., Chen, H.-W., & Bloom, J. S. 2006, ApJ, 648, 95
- Prochaska, J. X., et al. 2007a, ApJS, 168, 231
- Prochaska, J. X., Chen, H.-W., Dessauges-Zavadsky, M., & Bloom, J. S. 2007b, ApJ, 666, 267
- Prochaska, J. X., Dessauges-Zavadsky, M., Ramirez-Ruiz, E., & Chen, H.-W. 2008, ApJ, 685, 344
- Sari, R., Piran, T., & Narayan, R. 1998, ApJ, 497, L17
- Savaglio, S. 2006, New Journal of Physics, 8, 195
- Savaglio, S., Fall, S. M., & Fiore, F. 2003, ApJ, 585, 638
- Savaglio, S., et al. 2012, MNRAS, 420, 627
- Schady, P., Savaglio, S., Krühler, T., Greiner, J., & Rau, A. 2011, A&A, 525, A113
- Sheffer, Y., Prochaska, J. X., Draine, B. T., Perley, D. A., & Bloom, J. S. 2009, ApJ, 701, L63
- Stratta, G., et al. 2009, A&A, 503, 783
- Tagliaferri, G., et al. 2005, Nature, 436, 985

Vreeswijk, P. M., et al. 2004, *A&A*, 419, 927

—. 2007, *A&A*, 468, 83

Watson, D., Hjorth, J., Fynbo, J. P. U., Jakobsson, P., Foley, S., Sollerman, J., & Wijers, R. A. M. J. 2007, *ApJ*, 660, L101

Watson, D., et al. 2013, *ApJ*, 768, 23

Whalen, D., Prochaska, J. X., Heger, A., & Tumlinson, J. 2008, *ArXiv e-prints*, 802

Willingale, R., et al. 2007, *ApJ*, 662, 1093

Woosley, S. E. 1993, *ApJ*, 405, 273

Woosley, S. E., & Heger, A. 2006, *ApJ*, 637, 914

Yoon, S.-C., & Langer, N. 2005, *A&A*, 443, 643

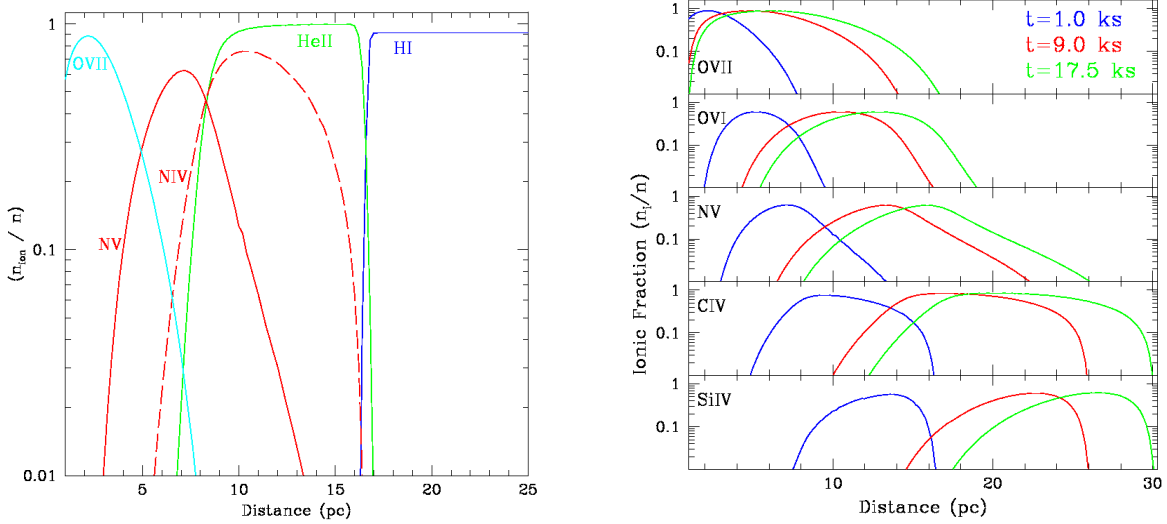


Fig. 1.— Time dependent photoionization model of the ISM surrounding GRB050730. The model was produced assuming the same conditions used by (Prochaska et al. 2008), including an homogeneous medium with number density $n(\text{H})=10 \text{ cm}^{-3}$. This comparison provides a test of the two codes and we find excellent agreement in the results. (Left): Ionization structure at observed time $t=1 \text{ ks}$. (Right): Ionization fractions for high ionization charge states as a function of distance at three different times, showing the time evolution of the ionization structure.

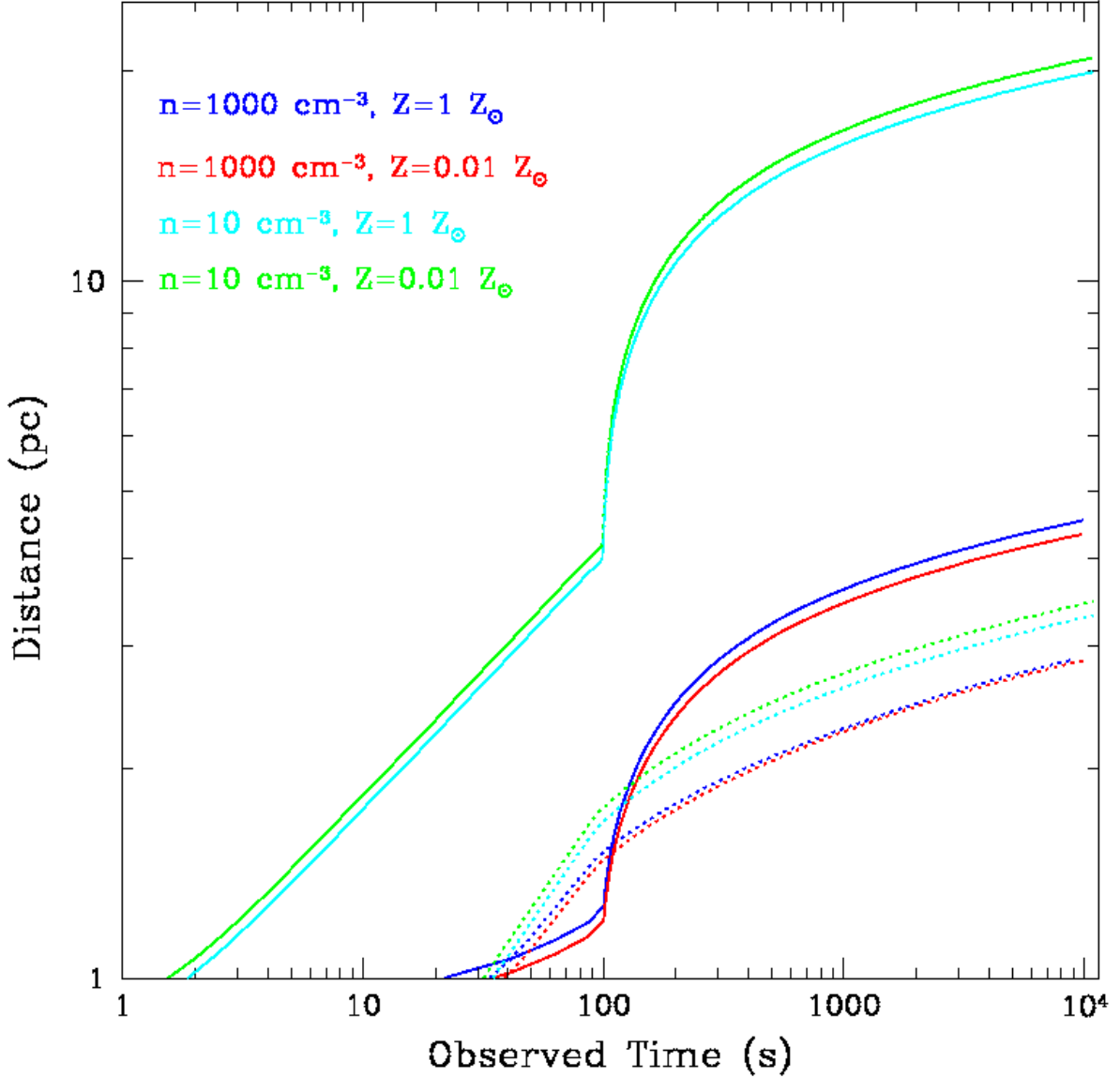


Fig. 2.— Time-dependent evolution of the ionization fronts of two transition regions: (i) solid curves trace the radius r_{HI} at which the gas has a 50% hydrogen neutral fraction; and (ii) dotted curves trace r_{OIX} , the radius at which the gas has 90% of its oxygen completely stripped of electrons. gas. The four models presented include two densities with two different metallicities each. We note very weak metallicity dependence on the results and find strong density variations only for r_{HI} . In general r_{HI} exceeds r_{OIX} as expected, but the prompt emission radiation field is sufficiently hard that does predict $r_{\text{OIX}} > r_{\text{HI}}$ for short times in some models.

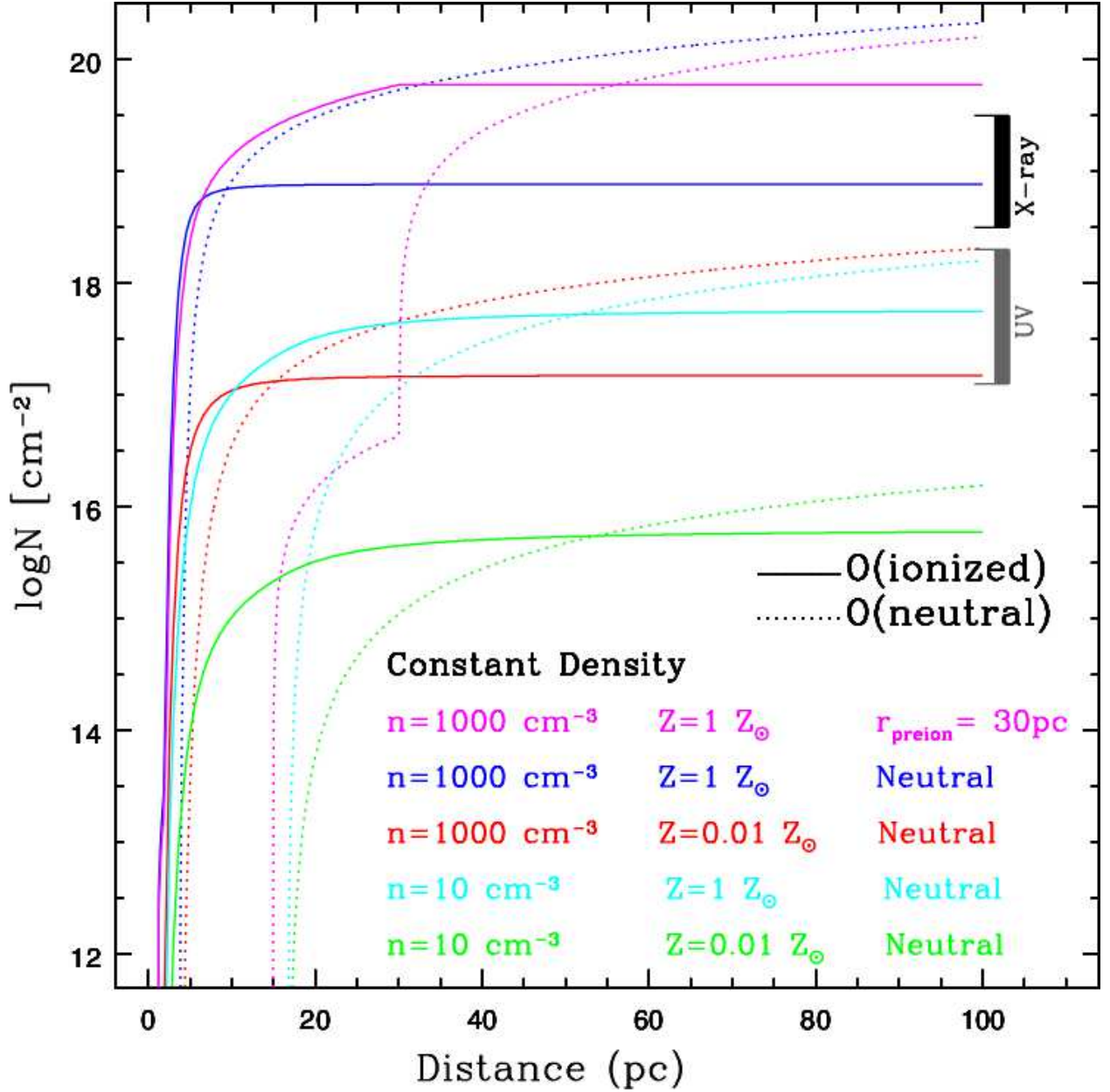


Fig. 3.— Predicted column densities from our time-dependent photoionization calculations of the circumbust medium at $t = 1000\text{s}$. These results are for a series of models assuming an homogenous medium, i.e. constant density and metallicity. Such models predict similar X-ray and optical/UV column densities. Generally, we find that the column densities of the gas which dominate the UV opacity are comparable to or even exceed those which are expected to produce the majority of X-ray opacity. Therefore, we consider these constant density models to be unviable.

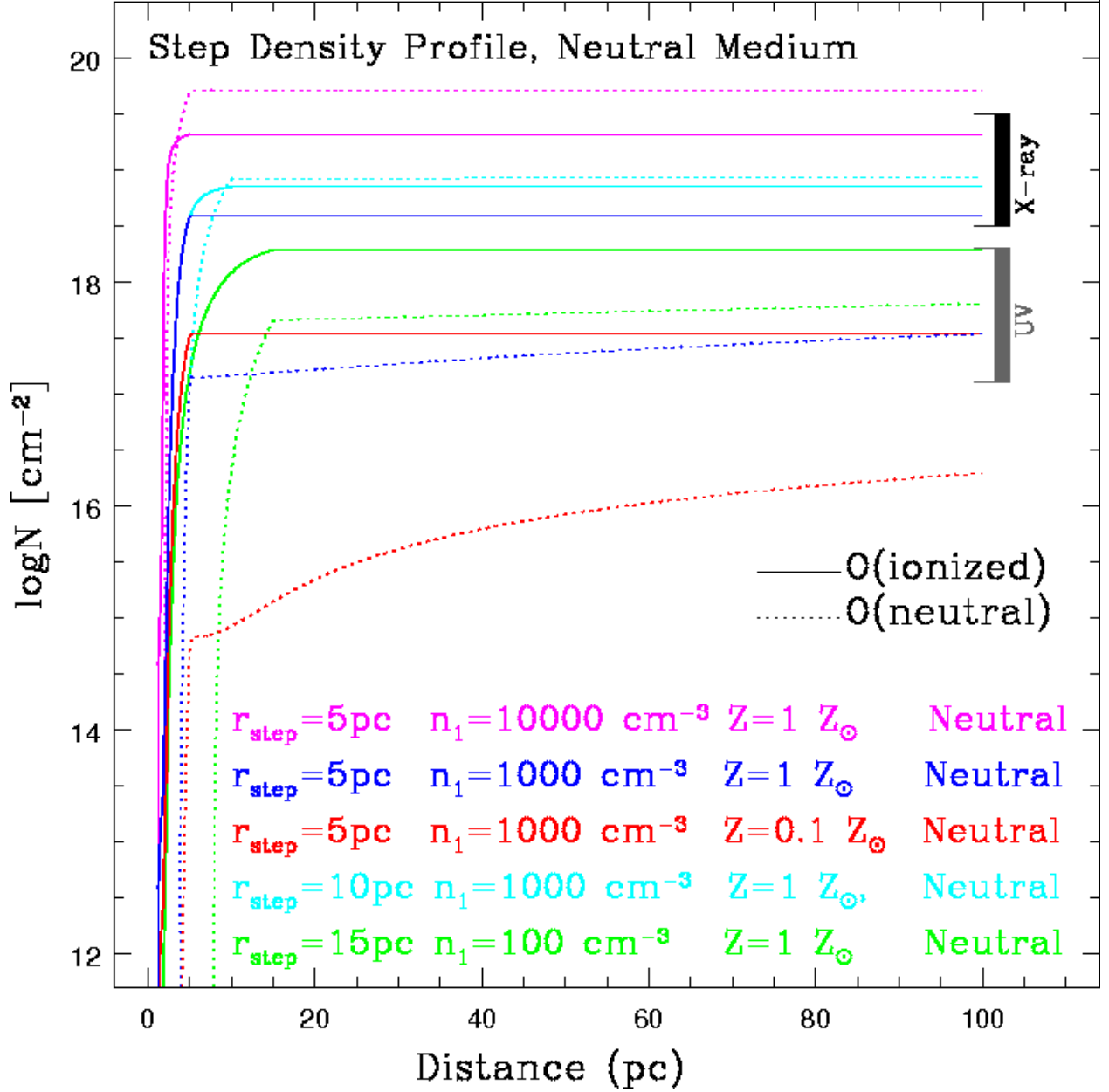


Fig. 4.— Predicted column densities from our time-dependent photoionization calculations of the circumbust medium at $t = 1000\text{s}$. The results are for models consisting of strong gradients of density between the regions close to the burst location (n_1) and the ISM ($n_2 = 1 \text{ cm}^{-3}$). A neutral medium prior to the burst is considered. Only models where the size of the dense regions is comparable to the ionization front can produce large X-ray to optical/UV column density ratios (e.g. $r_{\text{step}} = 5 \text{ pc}$, blue-colored curve).

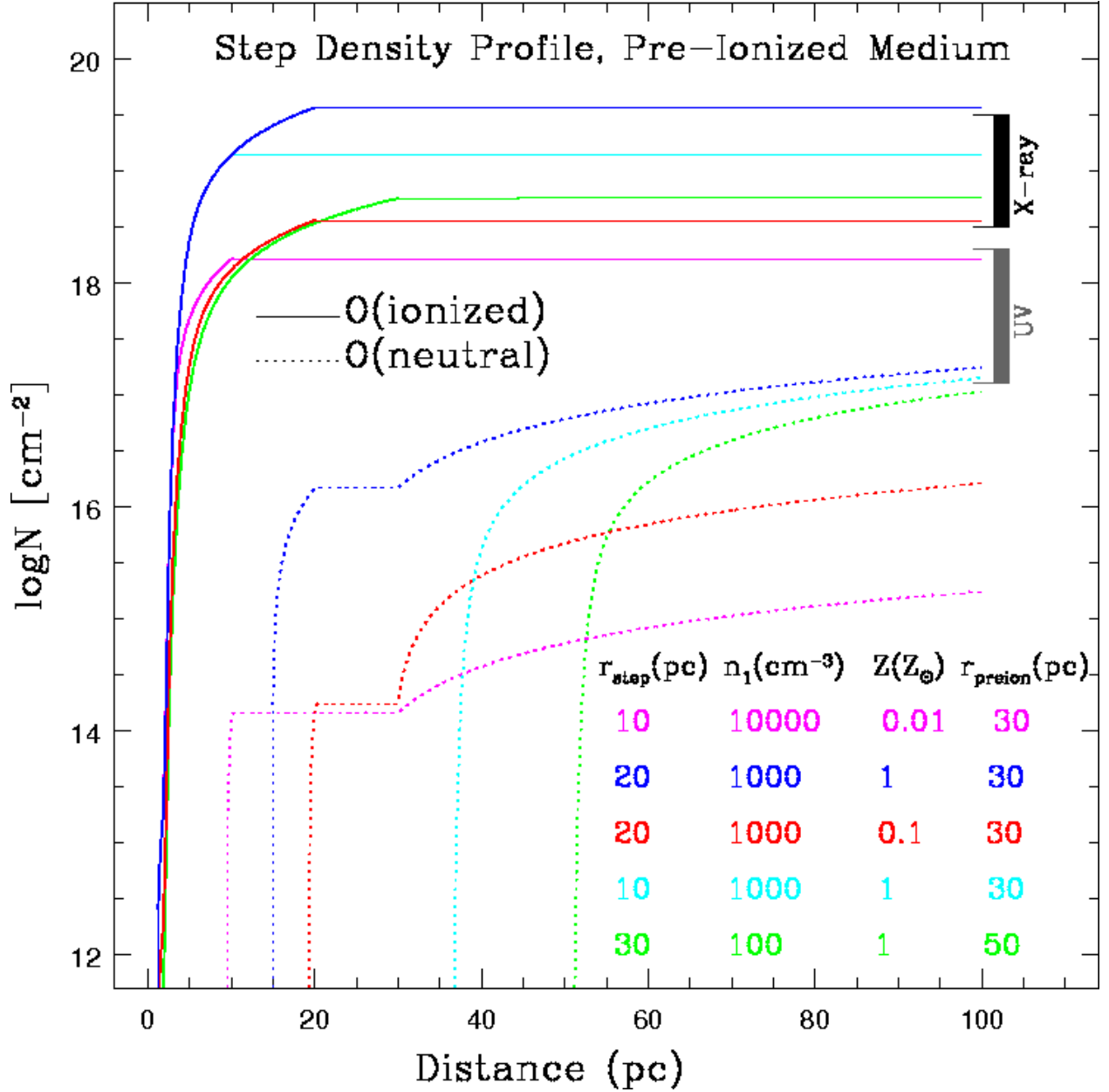


Fig. 5.— Predicted column densities by our time-dependent photoionization calculations of the circumbust medium at $t = 1000\text{s}$. These curves show the results for models consisting of strong gradients of density between the regions close to the burst location (n_1) and the ISM ($n_2 = 1 \text{ cm}^{-3}$) and also impose a pre-ionized medium where the gas within r_{preion} has been ionized to have a H neutral fraction $f(\text{HI}) = 10^{-5}$. All these models are able to explain the large X-ray columns, as well as the ‘excess’ with respect to the optical/UV values, as required by the observations. This is provided that $r_{\text{preion}} = 30 \text{ pc}$.

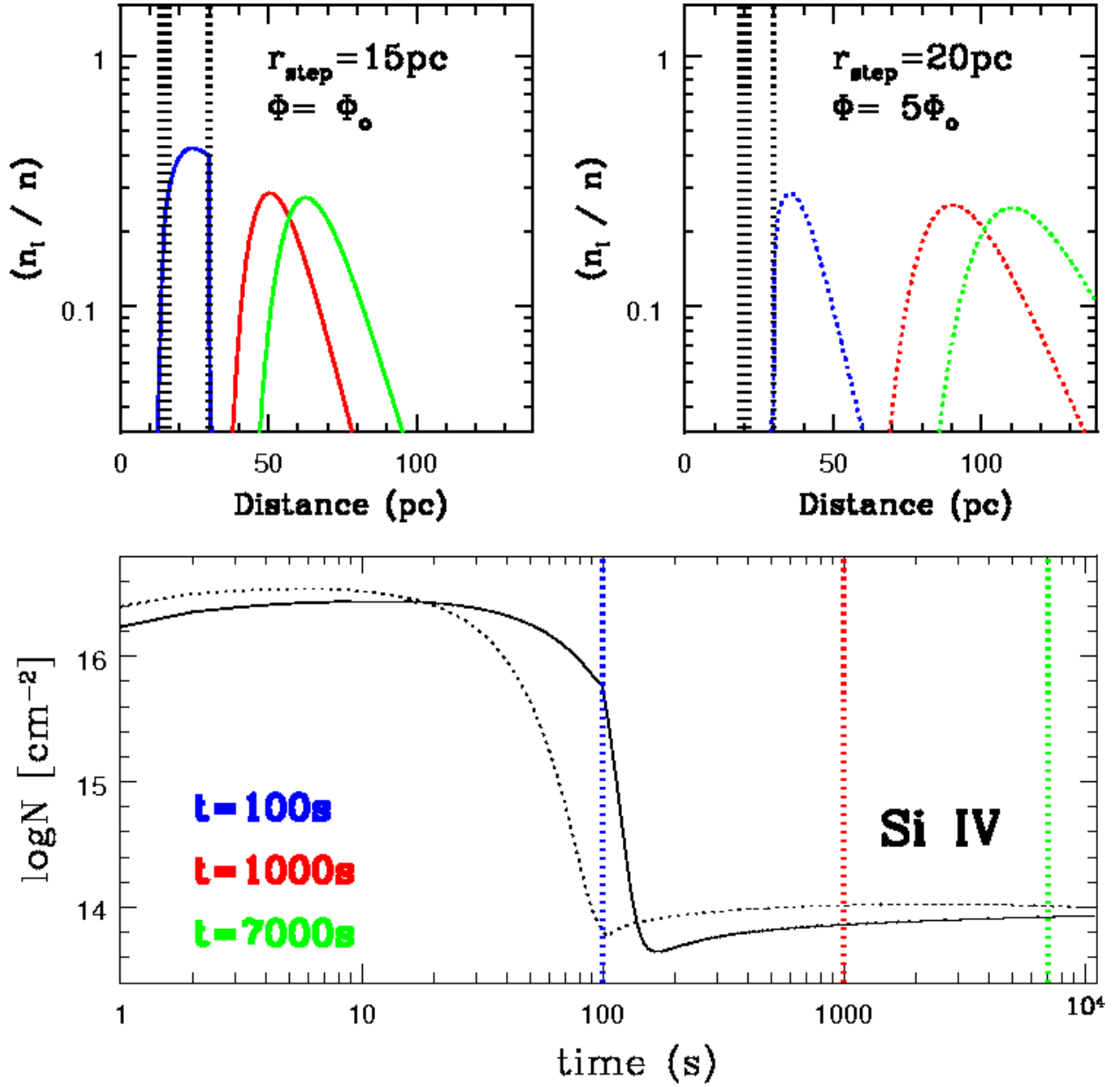


Fig. 6.— Time evolution of Si IV. The upper panels show the spacial distribution of the fraction of Si IV as a function of distance to the location of the burst, at three different times after the event. Two models are presented consisting on a step function with $n=10^3 \text{ cm}^{-3}$, and $Z=0.1 Z_{\odot}$. The models further assume a pre-ionized medium with $r_{\text{preion}} = 30 \text{ pc}$. The left panel shows a model with $r_{\text{step}} = 15 \text{ pc}$, and 2×10^{61} ionizing photons (our fiducial GRB). The right panel considers a case with $r_{\text{step}} = 20 \text{ pc}$, and five times more ionizing photons. The lower panel presents the column densities of Si IV as a function of time for the two models. The vertical color lines mark the ionization distributions at the times presented in the upper panels.

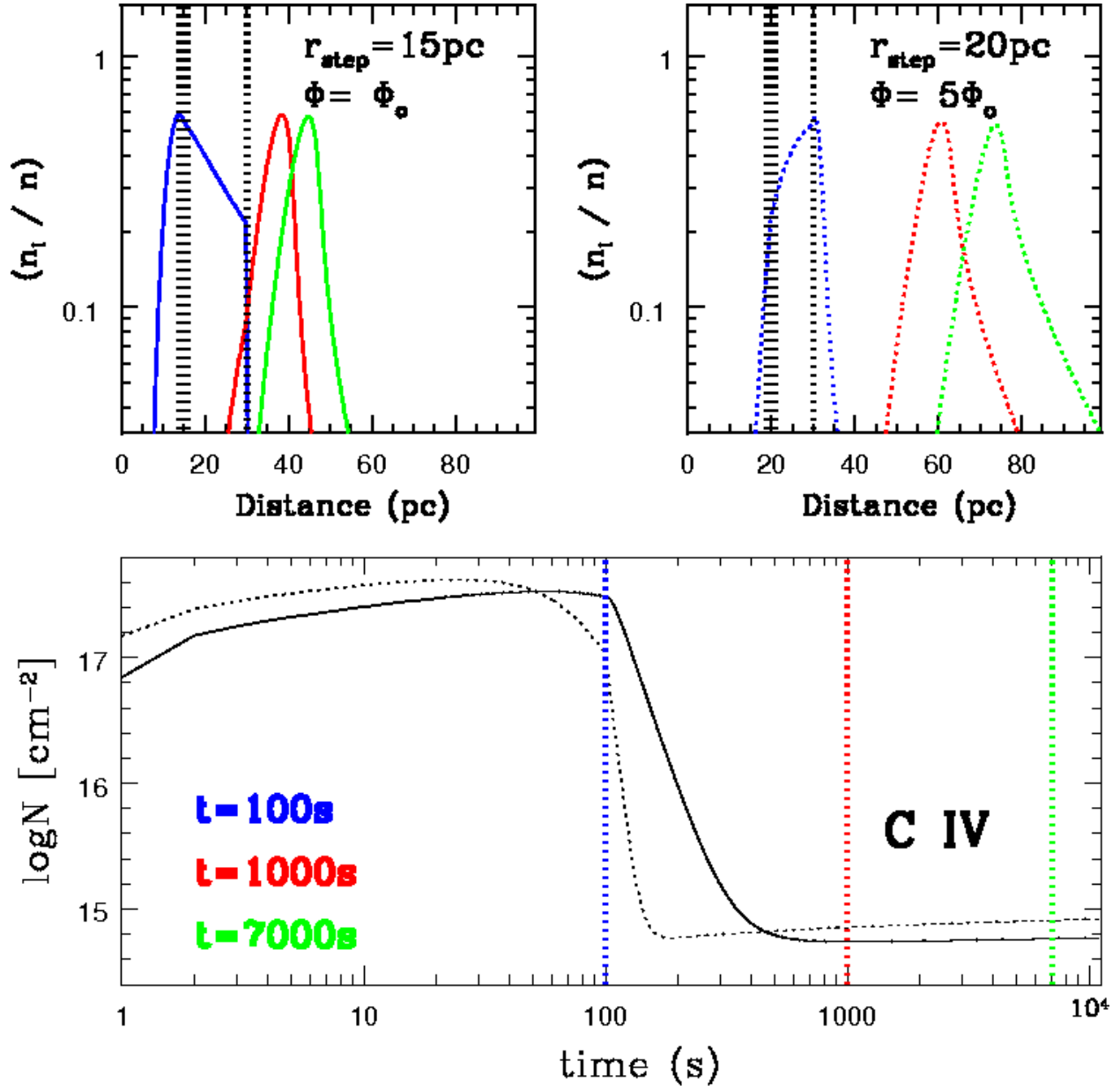


Fig. 7.— Time evolution of the fractional abundance and column density of C IV. Models and labels as in Fig. 6.

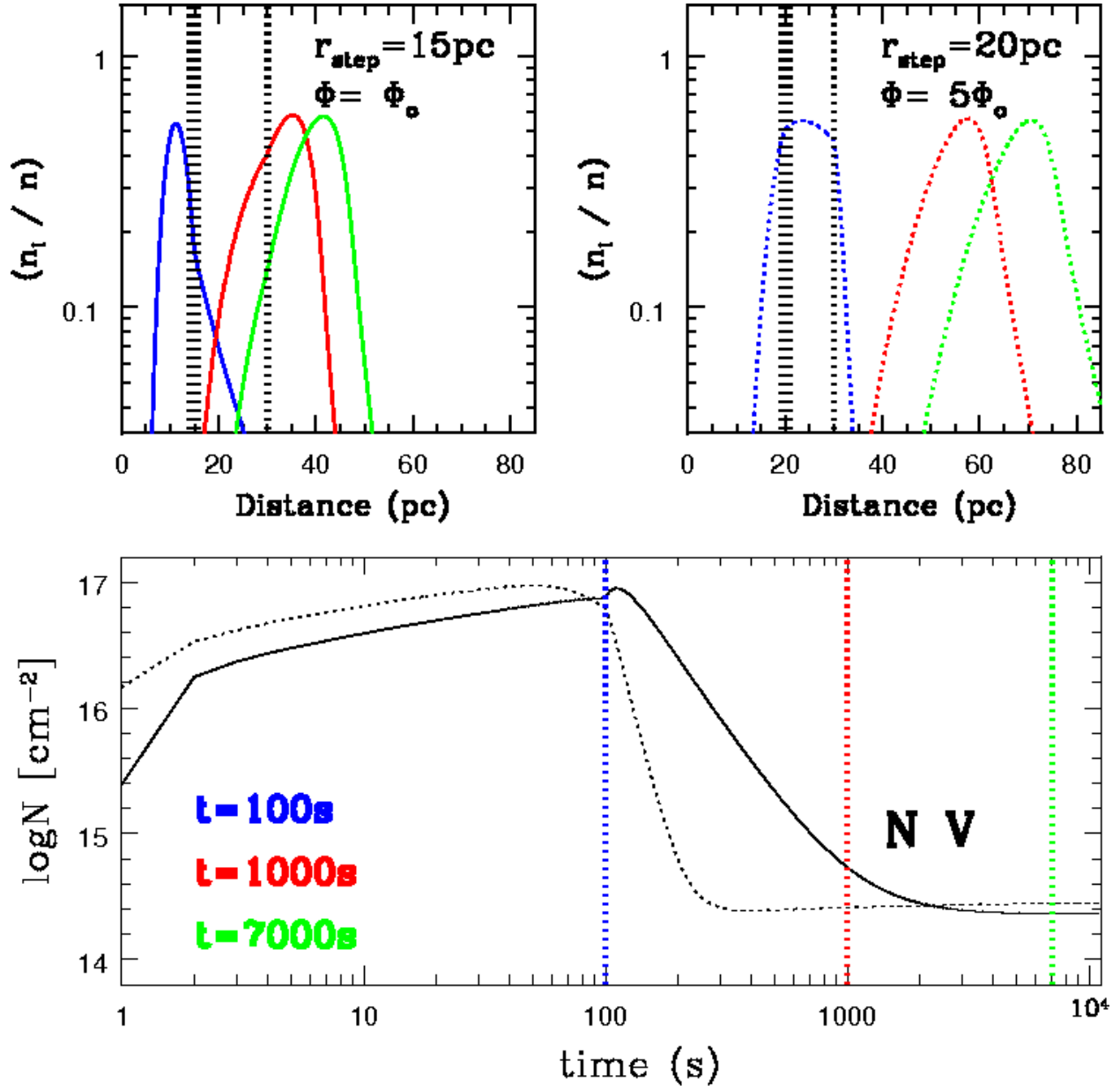


Fig. 8.— Time evolution of the fractional abundance and column density of N V. Models and labels as in Fig. 6

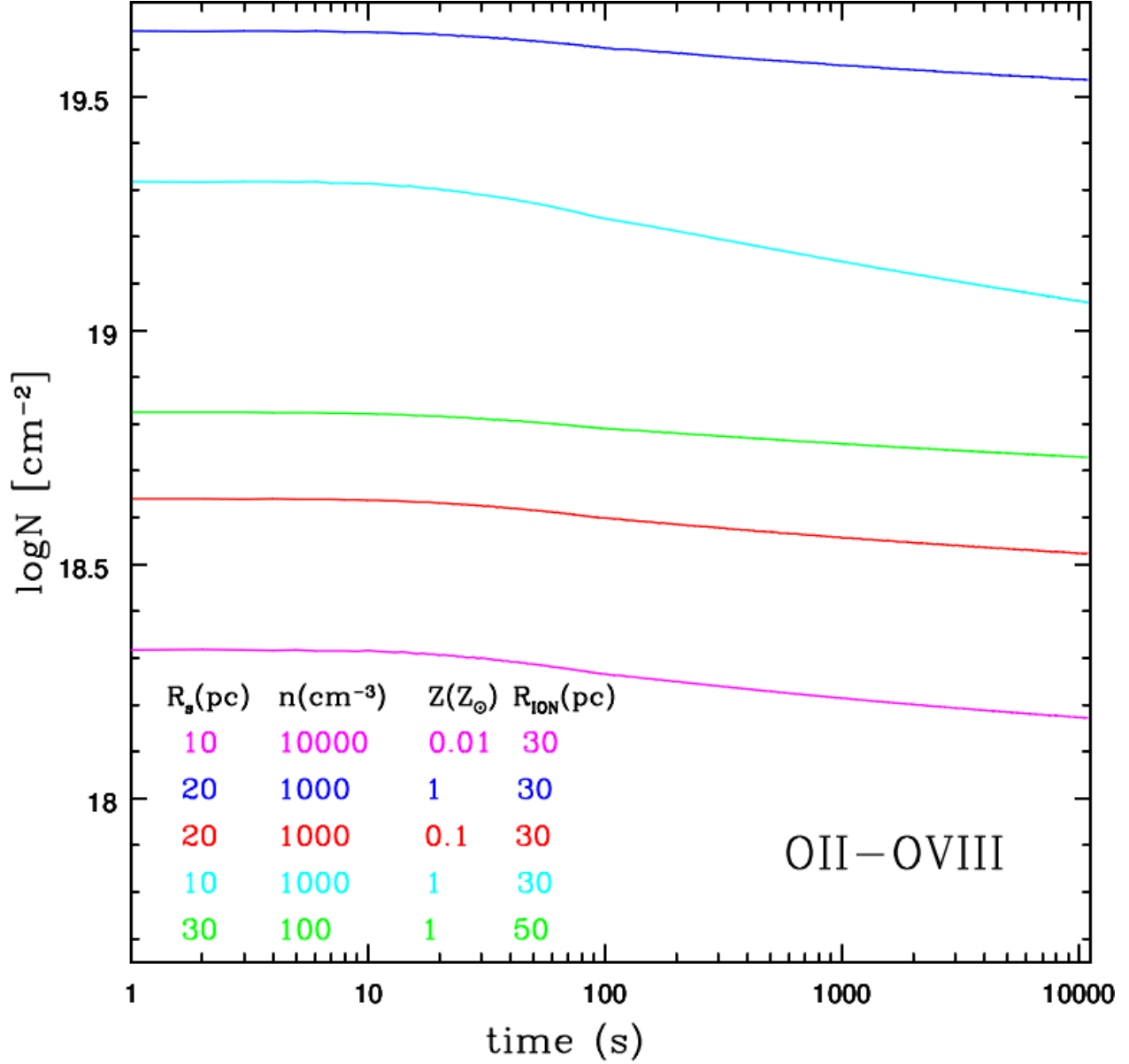


Fig. 9.— Time evolution of the total X-ray column densities produced by different step function models of the circumbust medium. Pre-ionization is assumed, with $r_{\text{preion}} = 30$ pc. Only integrated column densities for charge states OII to OVIII, as these are the ones driving the X-ray opacity. Only mild variations are expected.